optimal to induce any appreciable effect in the case of tea. This is in agreement with a few reports on other crops, wherein it was shown that the GA_3 effect is concentration and species-dependent[12]. The Ci/g_s values were relatively low in all GA_3-treated plants than that of control plants (Table 1), suggesting that the hormone-treated plants fix carbon efficiently at a given stomatal conductance, supporting our earlier findings in a few crop species[5–7].

The intrinsic carboxylation efficiency (dA/dCi) of control tea plant was 0.43 μmol $CO_2\ m^{-2}\ s^{-1}\ ppm^{-1}$. The dA/dCi of 50, 100 and 150 ppm GA_3-treated plants was 0.51, 0.56 and 0.61 μmol $CO_2\ m^{-2}\ s^{-1}\ ppm^{-1}$, indicating an apparent improvement in intrinsic carboxylation efficiency of 9, 19 and 30% respectively.

Ci/g_s showed a significant inverse relationship with dA/dCi in our study (Figure 1), which is in corroboration with our earlier findings in other crop species like sunflower, groundnut and cowpea[5,13,14]. A reduction in Ci levels can be expected either when the g_s is low or when the efficiency of carbon assimilation by the RuBisCO is high[14]. At a given g_s, therefore, variations in Ci are predominantly a function of carbon assimilatory capacity[13,14].

One of the formative effects of GA_3 has been on cell elongation, thereby maintaining cell turgidity[12]. The turgidity induces more cell growth leading to improvement of carbon exchange to water vapour ratio. In other words, to a given input of water, carbon assimilation would increase and hence the intrinsic water-use efficiency[13–17]. Steady tissue water status also improves the activities of photosynthetic carbon assimilatory enzymes, leading to efficiency of carbon fixation[12]. The increased efficiencies in water use and carboxylation in the case of tea plants treated with GA_3 in the present experiment might be a result of any one or collective effects of these physiological functions. This aspect needs to be re-examined by determining the content and activity of photosynthetic carbon assimilatory enzymes.

1. Assmann, S. M., *Plant Cell Environ.*, 1999, **22**, 629–637.
2. Cousson, A., *Plant Cell Environ.*, 2000, **23**, 487–495.
3. El-Sharkawy, M. A. and Cock, J. H., *Crop. Sci.*, 1983, **24**, 497–500.
4. von Caemmereer, S., Lawson, T., Oxborough, K., Baker, N. R., Andrews, T. J. and Raines, C. A., *J. Exp. Bot.*, 2004, **55**, 1157–1166.
5. Sheshshayee, M. S., Krishnaprasad, B. T., Nataraj, K. N., Prasad, T. G., Shankar, A. G. and Udayakumar, M., *Curr. Sci.*, 1996, **70**, 671–674.
6. Krishnaprasad, B. T., Sheshshayee, M. S., Nataraj, K. N., Prasad, T. G., Shankar, A. G. and Udayakumar, M., *Curr. Sci.*, 1996, **70**, 675–680.
7. Bindumadhava, H., Ph D thesis, University of Agricultural Sciences, Bangalore, 2000.
8. Bindumadhava, H., 2007 (in press).
9. Sharma, N., Bindumadhava, H., Joshi, M. K. and Prasad, T. G., 2007 (in press).
10. Mohotti, A. J. and Lawlor, D. W. J., *J. Exp. Bot.*, 2002, **53**, 313–322.
11. Raj Kumar, R., Burman, T. S. and Saikia, J. K., *Photosynthetica*, 1998, **35**, 41–46.
12. Tiaz and Zieger, *Textbook on Plant Physiology*, 2004, 3rd edn.
13. Bindumadhava, H., Sheshshayee, M. S., Shashidhar, G., Prasad, T. G. and Udayakumar, M., *Curr. Sci.*, 2005, **89**, 1256–1258.
14. Sheshshayee, M. S., Bindumadhava, H., Shanker, A. G., Prasad, T. G. and Udayakumar, M., *J. Plant Biol.*, 2003, **30**, 253–268.
15. Debabrata Ray, Sheshshayee, M. S., Mukhopadhyay, K., Bindumadhava, H., Prasad, T. G. and Udaya Kumar, M., *Biol. Planta.*, 2003, **46**, 251–256.
16. Kramer, P. J., *Adaptation of Plant to Water and High Temperature Stress* (eds Turner, N. C. and Kramer, P. J.), John Wiley, New York, 1980, pp. 7–20.
17. Angus, J. F. and van Jerzog, H., *Agron. J.*, 2001, **93**, 290–298.

ACKNOWLEDGEMENTS. We thank Drs G. M. Hegde, Chandramouli, Uma Shanker, Vilas Sinkar and Shovan Ganguli for help in conducting this work at HLL Stanmore Estate, Coimbatore. The project grant provided by the HLRC, Bangalore is acknowledged.

Received 11 July 2006; revised accepted 26 April 2007

H. BINDUMADHAVA[1,3,*]
T. G. PRASAD[1]
M. K. JOSHI[2]
N. SHARMA[2,3]

[1]*Department of Crop Physiology, University of Agricultural Sciences, GKVK Campus, Bangalore 560 065, India*
[2]*Hindustan Lever Research Centre, Bangalore 560 066, India*
[3]*Present address: ITC R&D Centre (Agri-Sciences), ITC Ltd, Hyderabad 500 034, India*
**For correspondence.*
e-mail: bindu.madhava@itc.in

Utility of OCEANSAT-1 OCM data in deciphering Antarctic features

The Antarctic ice (sea ice, icebergs, continental ice sheet) plays a significant role in determining the global climate. Remote sensing techniques are an obvious means to monitor and study the inaccessible region of the icy continent. Passive microwave remote sensing has been extensively used to monitor the extent, seasonal variation and secular trends of sea ice, information about icebergs, continental ice and geomorphic features of the Antarctic region[1–3]. However, due to low resolution, retrieving information about the small-scale features of the area is not possible. Therefore, optical remote sensing could emerge as a useful tool for detailed study at micro level, mainly due to its high resolution. In the Antarctic region long polar nights, extreme weather conditions and presence of clouds restrict the utility of optical remote sensing. Accordingly, in Antarctica optical remote sensing techniques can only be applied during austral summer when days are bright and sunny, and the sky is cloud-free.

In view of the above, data from Ocean Colour Monitor (OCM) sensor (which is an optical remote sensing sensor) of OCEANSAT-1 have been used in the present study to highlight distinct geological and geomorphic features. The Indian remote sensing satellite (IRS-P4), renamed later as OCEANSAT-1, was launched on 26 May 1999, on-board the indigenously developed Polar Satellite Launch Vehi-

cle. It carried two payloads: (i) the OCM, mainly for biological remote sensing of the oceans, and (ii) the Multi-frequency Scanning Microwave Radiometer to study physical parameters of the ocean and the overlying atmosphere (Figure 1).

OCEANSAT-1 was placed in a near-circular, sun-synchronous polar orbit at an altitude of 720 km. The satellite crosses the equator in the descending node at 12 ± 10 min. To attain a frozen perigee orbit, approximate orbit manoeuvres were carried out to ensure constant scale variations at any given latitude. The track was controlled within ±1 km of the reference ground trace pattern. The satellite takes the observation of the whole globe with a repeat cycle of two days[4].

The OCM is a solid-state camera operating at eight narrow spectral bands in the visible and near infrared parts of the electromagnetic spectrum. This payload works on the concept of push-broom imaging mechanism using a linear array of charge coupled devices. The instantaneous ground field of view of the instrument is 360 m, having a swath width of 1420 sq. km. To avoid the sun glint depending on the season, the electro-optic module has the provision to tilt the camera by ±20° alongtrack direction. The signal from the oceans constitutes a small fraction of the total radiance, reaching the sensor aperture and the rest is contributed by the scattered radiation from the atmosphere. OCM has a 12-bit radiometric precision to cover the entire dynamic range of the observations from ocean to land. It also has adequate signal-to-noise ratio at any signal condition. The major specifications of OCM are given in Table 1.

For the present purpose we have used OCM data of all bands, except band C1 (Table 2). In spite of the fact that OCM has narrow spectral channels for estimation of ocean colour parameters, it provides visible band images with good signal-to-noise ratio, particularly over the high reflecting ice surface. Determination of latitude and longitude on the basis of path and row of the scene was done by choosing the data or observing the 7/21 path and row of OCM data, which were specified by the National Remote Sensing Agency, Hyderabad. On the basis of the obtained path, the location of the Indian permanent base at Antarctica, namely Maitri (70°05′S lat. and 11°47′E long.) was deciphered on the scene. The data were processed with the help of ERDAS image processing software. Initially the full scene of 7 path was viewed, which was matched with the ETOPO map of Antarctica (at a resolution of 5′ × 5′), to confirm the deciphered location. Subsequently, from the full scene of 7/21 path and row, the image of the area of our interest around Maitri was extracted by subsetting of the images using subset techniques in ERDAS imagine. The image was further enhanced using the image enhancement technique of ERDAS. Enhancement provides important features of raw, remotely sensed data more interpretable by the human eye. Enhancement techniques are often preferred to the classification techniques for feature extraction, studying and locating areas or objects on the ground and deriving useful information from the images. Operations performed in the frequency (Fourier) domain can be visualized in the context of the familiar convolution function. The mathematical basis of this inter-relationship is the convolution theorem, which states that a convolution operation in the spatial domain is equivalent to a multiplication operation in the frequency domain:

$$g(x, y) = h(x, y) \text{ þ } f(x, y) \text{ þ } G(u, v) = H(u, v) \text{ þ } F(u, v),$$

where $f(x, y)$ is the input image, $h(x, y)$ the position invariant operation (convolution kernel), $g(x, y)$ the output image, and G, F, H are the Fourier transforms of g, f, h. High-pass, low-pass, high-frequency indicate that these convolution functions derive from the frequency domain, low-pass filtering.

The simplest example of this relationship is the low-pass kernel. This name is derived from a filter that would pass low frequencies and block (filter out) high frequencies. In practice, this is easily achieved in the spatial domain by the $M = N = 3$ kernels:

$$\begin{bmatrix} 1 & 1 & 1 \\ 1 & 1 & 1 \\ 1 & 1 & 1 \end{bmatrix}.$$

As the size of the image, particularly the size of the low-pass kernel increases, the calculation becomes more time-consuming. Depending on the size of the input image

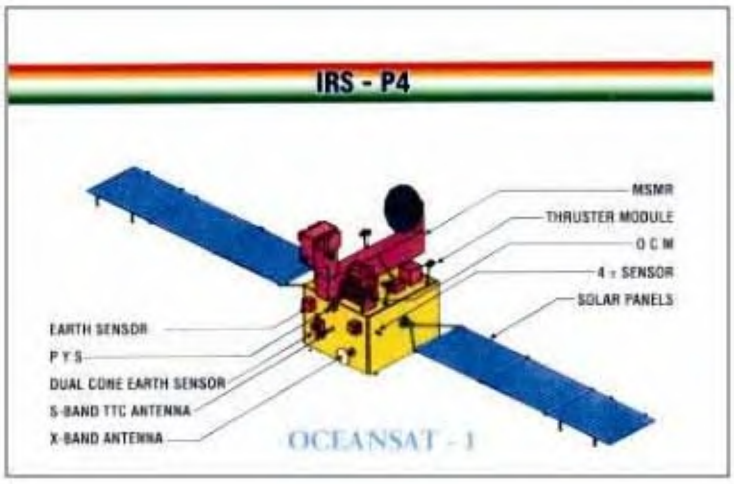

Figure 1. OCEANSAT-1 in space.

Table 1. Major specifications of OCM

Parameter	Specifications
IGFOV at 720 km altitude	360 m (across track) × 250 m (along track)
Swath	1420 km
No. of spectral bands	8
Spectral range	402–885 nm
Signal quantization	12-bit
Camera MTF (at Nyquist frequency)	>0.2
Alongtrack steering	+20°, 0°, –20°
Data rate	20.8 Mbits/s

Table 2. Spectral bands of OCM and their applications

Spectral bands	Wavelength range (in nm)	Applications
C1	402–422	Yellow substance and turbidity
C2	433–453	Chlorophyll absorption maxima
C3	480–500	Chlorophyll and other pigments (≤1.5 mg/m^3)
C4	500–520	Chlorophyll and other pigments (≥1.5 mg/m^3)
C5	545–565	Suspended sediments (away from chlorophyll and Gelbstoff)
C6	660–680	Second chlorophyll absorption maxima
C7	745–785	O_2 absorption *R*-branch
C8	845–885	Aerosol optical thickness

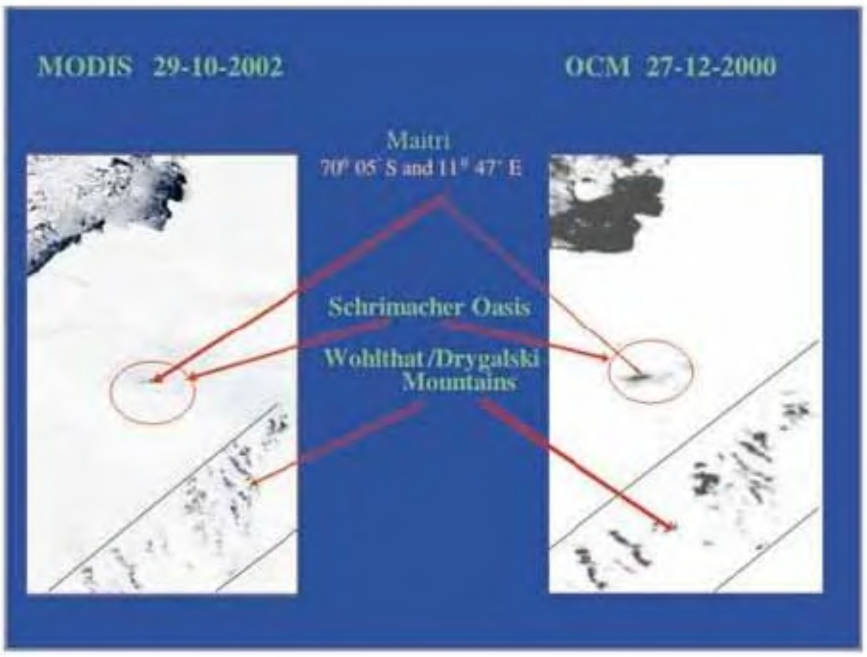

Figure 2. Validated OCM image with MODIS.

and that of the kernel, it can generate faster a low-pass image via Fourier processing. We applied in-built low-pass filtering using ERDAS imagine software. The final image generated by the above techniques from OCM (band 2) was compared with the same area image of MODIS using TIR channel. The final enhanced image revealed ice features, including mountains.

The inferences drawn from this study are in agreement with the same scene of the standard MODIS[5–7]. Images thus obtained by OCM (on 27 December 2000) and MODIS (on 29 October 2000) were brought to the same scale for validation purpose. The validated images of the identified site (Maitri station) are given in Figure 2, which clearly shows the area around the Indian research base, Maitri. Under 360 m resolution, visible and near infrared wavelength Maitri appears as a black dot. Furthermore, around Maitri signatures of Schrimacher Oasis, and Wohlthat/Drygalski Mountains could also be traced. It depicts the observed features, after applying the low-pass filter to the second band.

In summary, the preliminary results on the utility of OCM data in deciphering Antarctic features are encouraging. However, further detailed studies and analyses of OCM data are required to identify various ice features near the coasts and around Maitri. The combination of thermal channels in the MODIS data may bring more information, such as ice surface temperature, elevation of ice aggregation over Maitri, thermal behaviour of ice (which may be a proxy to study the multiyear ice) and classification of Antarctic ice/sea ice, etc. Since OCM does not carry thermal channels, there is a need to develop methods by combining both these sensors for further refinement of the result.

1. Bhandari, S. M., Dash, M. K., Vyas, N. K., Khare, N. and Pandey, P. C., *Advances in Marine and Polar Science* (eds Sahoo, D. and Pandey, P. C.), A. P. H. Publishing Corporation, New Delhi, 2002, pp. 423–443.
2. Vyas, N. K., Dash, M. K., Bhandari, S. M., Khare, N., Mitra, A. and Pandey, P. C., *Int. J. Remote Sensing*, 2003, **24**, 2277–2287.
3. Vyas, N. K., Bhandari, S. M., Dash, M. K., Pandey, P. C., Khare, N., Khanolkar, A. and Sharma, N., *An Atlas of Antarctic Sea–Ice from Oceansat – MSMR data (June 1999–September 2001)*. A joint publication by ISRO, Ahmedabad and NCAOR, Goa, 2004, p. 61.
4. ISRO, IRS-P4 MSMR data products format. DOC.NO.ISRO-SAC-IRS-P4-DP/MSMR/FORMAT/VERSION2.0/2/99, 1999, p. 31.
5. Hall, D. K., Kelly, R. E. J., Riggs, G. A., Chang, A. T. C. and Foster, J. L., *Ann. Glaciol.*, 2002, **34**, 24–30.
6. Klein, A. G. and Stroeve, J., *Ann. Glaciol.*, 2002, **34**, 45–52.
7. Zhou, X. and Li, S., *Int. J. Remote Sensing*, 2003, **24**, 5011–5032.

Received 6 January 2006; revised accepted 2 April 2007

N. KHARE[1,*]
N. SHARMA[1]
S. M. BHANDARI[2]
N. K. VYAS[2]

[1]*National Centre for Antarctic and Ocean Research, Headland Sada, Vasco-da-Gama, Goa 403 805, India*
[2]*Space Applications Centre (ISRO), Ahmedabad 380 015, India*
**For correspondence.*
e-mail: nkhare@ncaor.org